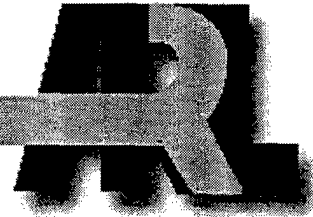


ARMY RESEARCH LABORATORY



Comparison of Numerical Flow Field Predictions for Army Airdrop Systems

Jubaraj Sahu
Harris L. Edge
Karen R. Heavey
Keith R. Stein
Richard J. Benney
Sukumar R. Chakravarthy

ARL-TR-1983

MAY 1999

19990618 191

DTIC QUALITY INSPECTED 4

Approved for public release; distribution is unlimited.

The findings in this report are not to be construed as an official Department of the Army position unless so designated by other authorized documents.

Citation of manufacturer's or trade names does not constitute an official endorsement or approval of the use thereof.

Destroy this report when it is no longer needed. Do not return it to the originator.

Army Research Laboratory

Aberdeen Proving Ground, MD 21005-5066

ARL-TR-1983

May 1999

Comparison of Numerical Flow Field Predictions for Army Airdrop Systems

Jubaraj Sahu
Harris L. Edge
Karen R. Heavey
Weapons & Materials Research Directorate, ARL

Keith R. Stein
Richard J. Benney
Army Soldier and Biological Chemical Command

Sukumar R. Chakravarthy
Metacomp Technologies, Inc.

Approved for public release; distribution is unlimited.

Abstract

A computational study has been performed to determine the aerodynamics of Army airdrop systems using computational fluid dynamics (CFD). The validation of flow field predictions from CFD software packages for airdrop systems is difficult because comprehensive experimentally obtained data are lacking. This is especially true for real systems because obtaining desired flow field data during a test is not practical or possible with available technologies. This report examines the results of predictions from two separate CFD codes for the same airdrop systems as an initial step toward validating high performance computing software for modeling airdrop systems. Numerical results have been obtained on two airdrop systems used by the U.S Army: the T-10 personnel system (no payload) and the G-12 cargo system with and without a payload. The two software packages used for the comparisons are a CFD code that employs a stabilized semi-discrete finite element formulation of the incompressible Navier-Stokes equations and CFD++, a commercially available code. For this numerical experiment, computed unsteady flow fields were obtained with the same unstructured mesh, and predicted flow fields were compared. Similarities and discrepancies in the comparisons are highlighted, and conclusions are drawn from these results.

TABLE OF CONTENTS

	<u>Page</u>
LIST OF FIGURES	v
1. INTRODUCTION	1
2. NUMERICAL TECHNIQUES	2
2.1 Finite Element Flow Solver	2
2.2 CFD++ Solver	3
3. RESULTS	5
4. CONCLUDING REMARKS	15
REFERENCES	17
DISTRIBUTION LIST	19
REPORT DOCUMENTATION PAGE	23

INTENTIONALLY LEFT BLANK

LIST OF FIGURES

<u>Figure</u>		<u>Page</u>
1.	Computational Surface Mesh for T-10	5
2.	Slice of Computational Mesh in x-z	6
3.	Snapshot of Predicted T-10 Flow Field	6
4.	Pressure Contours on the Lower Surface	7
5.	Pressure Contours on the Upper Surface	7
6.	Computed Pressure Contours	8
7.	Computed Velocity Magnitude Contours	9
8.	Computed Velocity Vectors	9
9.	Computed Pressure Comparisons	10
10.	Velocity Magnitude Comparisons	10
11.	Computed Results With One-Equation Model	11
12.	Comparison of Computed Results	11
13.	Time History for Drag for T-10 Parachute	12
14.	Mesh for G-12 Parachute Without Payload	13
15.	Computed Pressure Contours (coarse mesh)	13
16.	Computed Pressure Contours (fine mesh)	14
17.	Convergence of Drag for G-12 Canopy	14
18.	Mesh for G-12 Parachute With Payload	15
19.	Computed Pressures for G-12 With Payload	15

INTENTIONALLY LEFT BLANK

COMPARISON OF NUMERICAL FLOW FIELD PREDICTIONS FOR ARMY AIRDROP SYSTEMS

1. INTRODUCTION

The interaction between the parachute system and the surrounding flow field is dominant in most parachute operations, and thus the ability to predict parachute fluid-structure interaction (FSI) is necessary for an accurate prediction of parachute behavior. The U.S. Army is investing in developing tools to simulate parachute FSI. A computational tool that models the terminal descent characteristics of a single parachute and a cluster of parachutes is a technology that is needed by parachute designers and engineers. There has been a continuing effort between the U.S. Army Soldier and Biological Chemical Command, Soldier Systems Center (Natick, Massachusetts) and the U.S. Army Research Laboratory (ARL) (Aberdeen Proving Ground, Maryland) to develop this computational tool. The collaborative effort focuses on airdrop system modeling through a technology program annex. Because extensive experimental data are lacking, it is difficult to determine the accuracy of the predicted flow fields around parachutes. Also, a clear understanding of the wake flow field behind the parachute body for a single parachute, as well as clusters of parachutes, does not exist. Current cluster parachute systems are over-designed and often poorly optimized because the interacting flow fields associated with these parachute systems are not clearly understood.

The ultimate goal is to develop capabilities to model the airdrop system from the opening process to the final terminal descent. The opening process of the airdrop system is extremely complex and is not a current goal of this work. The emphasis here is on the numerical computational fluid dynamics (CFD) prediction of the flow over airdrop systems in the terminal descent phase. The ability to accurately simulate the flow field around a parachute is a complex problem. The aerodynamic characteristics associated with a single parachute or a cluster of parachutes in the terminal descent phase are extremely complex to model. The complexity arises largely from the fact that the flow field depends on the canopy shape, which itself depends on the flow field. A correct model must include the coupled behavior of the parachute system's structural dynamics with the aerodynamics of the surrounding flow field. A coupled model is required to determine the terminal descent characteristics of parachutes, including velocity, shape, drag, pressure distribution, and the other flow field characteristics.

As a starting point, the present research has focused on the use of CFD to gain a basic understanding of the aerodynamic interference flow fields associated with parachute clusters. Prior work included CFD modeling of single axisymmetric and three-dimensional (3-D) canopies.

In this case, CFD techniques were used to model a fixed shape single canopy in 3-D. The results were manually coupled to a static structural code that predicted the canopy shape based on a CFD-supplied canopy surface pressure distribution.[1,2] These solutions were obtained by using different numerical codes at ARL, and Natick provided good agreement of pressures on the parachute inner and outer surfaces. Again, no experimental data were available for comparison with the computed results. CFD modeling was then extended to include a cluster of three half-scale C-9 flat circular parachutes.[3] The rationale for choosing this configuration was to compare some aspects of the solutions to an experimental study of this cluster configuration during controlled conditions, recently completed by Lee, Lanza, and Buckley.[4]

This report describes the application of two separate CFD codes for the same airdrop system. A brief description of both numerical techniques is provided in the following section. For this numerical experiment, computed unsteady flow fields have been obtained with the same unstructured mesh, and predicted flow fields have been compared.

2. NUMERICAL TECHNIQUES

2.1 Finite Element Flow Solver

One strategy being employed to simulate parachute FSI uses the deforming-spatial-domain/stabilized space-time (DSD/SST) formulation [5,6] of the time-dependent, 3-D Navier-Stokes equations of incompressible flows. The DSD/SST procedure is well suited for problems involving changes in the shape of the spatial domain, such as those encountered during parachute FSI. This formulation has been well tested and applied to a large variety of fluid dynamics problems involving moving boundaries and interfaces. In the space-time formulation, the finite element interpolation functions vary both spatially and temporally, automatically accounting for changes in the spatial domain. Turbulent features of the flow are accounted for using a simple algebraic turbulence model. The formulation is stabilized against two types of instabilities that arise for advection-dominated flow [7] and for formulations with equal order interpolation functions for velocity and pressure.[8]

For the problems presented, our primary focus is on the time-dependent flow field surrounding the canopy of a U.S. Army T-10 system. For these simulations, we assume that the canopy is rigid, and thus there is no deformation of the spatial domain. Instead of the stabilized space-time formulation, we use a stabilized semi-discrete formulation of the 3-D Navier-Stokes equations of incompressible flows.[7] As in the space-time formulation, the semi-discrete formulation is stabilized against two types of instabilities. However, this formulation is adequate

for problems with no spatial deformations and is less computationally intensive than the space-time formulation. For the problems being considered, the fluid is assumed to be Newtonian, and the dynamic viscosity is modified locally using a Smagorinsky turbulence model.[9]

2.2 CFD++ Solver

The CFD++ code [10,11] incorporates the unified grid, unified computing, and unified physics methodologies developed by Metacomp Technologies. The unified grid methodology involves the unification of cell types and grid topologies. CFD++ is capable of handling a combination of hexahedral, tetrahedral, and triangular prism cells in 3-D; quadrilaterals and triangles in 2-D; and line elements in 1-D. Its bookkeeping and automatic zonal connectivity detection capabilities also unify the treatment of structured, unstructured, patched-aligned, and nonaligned grids. The unified computing aspects of CFD++ allow its portability on many computer platforms from the simple PC to the powerful massively parallel computers.

The initial development of CFD++ was for compressible flows. For compressible flows as well as low-speed incompressible flows, a preconditioning approach has been added. With CFD++, low-speed compressible flows can be simulated using both the compressible flow and the incompressible flow frameworks, which have been integrated in a unified fashion. Preconditioning normalizes the eigenvalues and achieves very good convergence rates for steady state problems. This is obtained by multiplying the time derivative vector of the variables by a preconditioning matrix [12,13]:

$$P^{-1}q_t + f_x + g_y + h_z = 0$$

Now if this is inverted, one obtains the following equation:

$$q_t + P(f_x + g_y + h_z) = 0$$

It is clear that this will change the eigenvalues and eigenvectors of the Jacobian matrices associated with preconditioned inviscid fluxes. This also destroys the correct transient and takes a different path to the correct steady state solution. Dual time-stepping techniques available in CFD++ can be used for transient problems.

For incompressible flow, density can be a function of temperature but not of pressure. This creates a problem if one is to use the traditional ways to update the conservation variables in the Navier-Stokes equations. Following the method proposed in Weiss and Smith [12], a new

set of variables is used in order to update the equations. Let us begin with the integral (conservation) form of the Navier-Stokes equations:

$$\frac{\partial}{\partial t} \iiint q dV + \iint [F - G] dA = 0$$

This can be rewritten as

$$\left(\frac{\partial q}{\partial Q} \right) \frac{\partial}{\partial t} \iiint Q dV + \iint [F - G] dA = 0$$

in which Q is the vector of primitive variables $(p, T, u, v, w)^T$. We now multiply the time derivative term by a preconditioning matrix so that the resulting eigenvalues of the inviscid terms are normalized. The eigenvalues of the preconditioned system are given by

$$u' - c' \quad u \quad u' + c'$$

in which

$$u = un_x + vn_y + wn_z$$

$$u' = u(1 - \alpha)$$

$$c' = \sqrt{\alpha^2 u^2 + U^2}$$

$$\alpha = \frac{(1 - \beta U^2)}{2}$$

$$\beta = \left(\rho_p + \frac{\rho_T}{\rho C_p} \right)$$

in which n_x , n_y , and n_z are the cell face normal, U is the preconditioning parameter, ρ_T and ρ_p are the derivative of density with respect to temperature and pressure, and C_p is the specific heat at constant pressure. If one starts with the nonconservation form of the equations, it can be easily shown that this preconditioning involves changing the ρ_p term in the first equation into $(I / U^2 - \rho_T / \rho C_p)$. This has the effect of changing the eigenvalues to the ones given previously.

The quantity U given in these equations is a reference velocity that is usually set to some factor of the local velocity and is the driving force behind the normalization of the eigenvalues. If one further analyzes the aforementioned eigenvalues for an incompressible constant density flow, one finds that β is zero and α is 1/2. Therefore, as long as U is of the same order as the local velocity, the eigenvalues all remain the same order as u .

3. RESULTS

The T-10 parachute is a 35-foot constructed diameter, flat extended skirt canopy consisting of 30 suspension lines. The G-12 parachute is a 64-foot constructed diameter, flat circular canopy consisting of 64 suspension lines. A structural dynamic finite element code was used to generate the predicted inflated shape of these two canopies.[14,15] The inflated shapes were used to construct the unstructured CFD meshes for each of these models. The unstructured 3-D volume meshes were generated with an automatic mesh generation software.[16] Since the thickness of the parachute is rather small, it is neglected. The parachute inner surface is first represented with an unstructured mesh (see Figure 1). The coordinates shown here are dimensionless. The vent opening of the T-10 parachute, as well as all the gores, can clearly be seen in this figure. The outer surface of the parachute is defined to be equivalent to the inner parachute surface. That is, the nodes on the outer surface of the parachute have the same coordinates as those of the matching inner surface. A slice of the full 3-D CFD mesh through the xz plane for the T-10 canopy is shown in Figure 2. It shows the clustering of the mesh points near the parachute and the wake region. Figure 3 shows the predicted flow field from the finite element code at a snapshot in time through a symmetrical cutting plane view of the T-10. The left-hand side of the figure shows the predicted pressure distribution and the unstructured mesh. The right-hand side of the figure shows the predicted velocity vectors and pressure distribution.

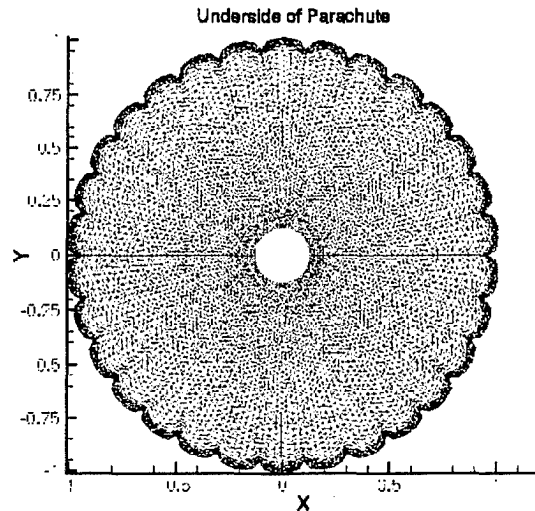


Figure 1. Computational Surface Mesh for T-10.

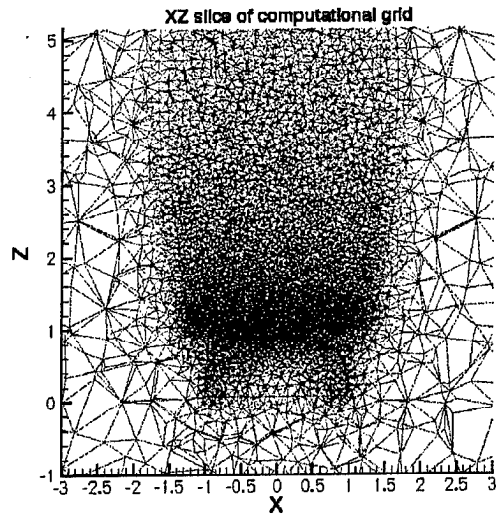


Figure 2. Slice of Computational Mesh in x-z.

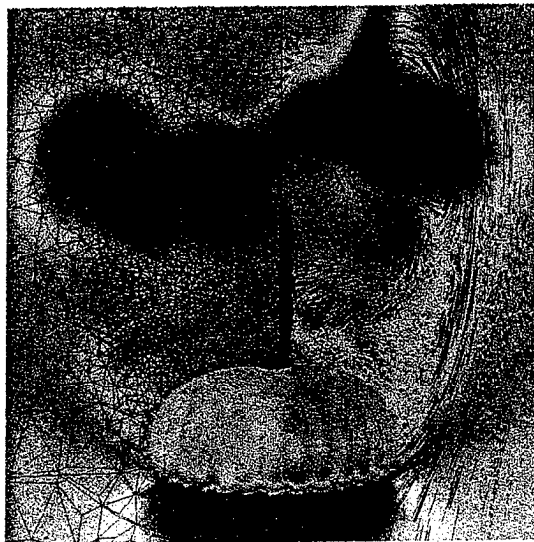


Figure 3. Snapshot of Predicted T-10 Flow Field.

The same unstructured grid was used in the CFD++ code to compute the flow around the T-10 parachute. The unstructured grid was converted from its initial format to CFD++ internal format. The parachute drop velocity at terminal descent corresponds to approximately a Mach number of 0.016 (or 18.0 feet per second). Computations were performed for the T-10 case using both one-equation and two-equation k-e turbulence models. Computed results were also obtained for laminar flow conditions for comparison. Figures 4 and 5 show the computed

pressure contours on the inside surface and outside parachute surface, respectively, at one instant in time. As seen in Figure 4, the computed inner surface pressures are high and the results indicate a fairly symmetrical flow field. The pressure contours on the outer parachute surface are clearly asymmetrical (see Figure 5), and in general, these pressures are lower than the computed pressures on the inner surface.

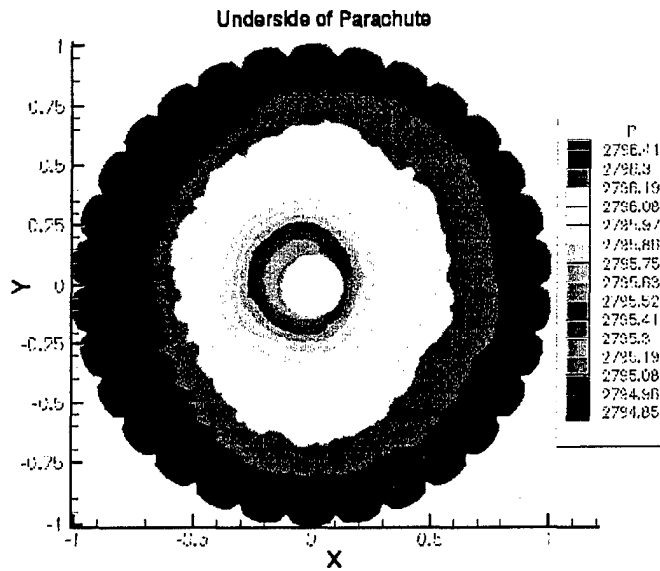


Figure 4. Pressure Contours on the Lower Surface.

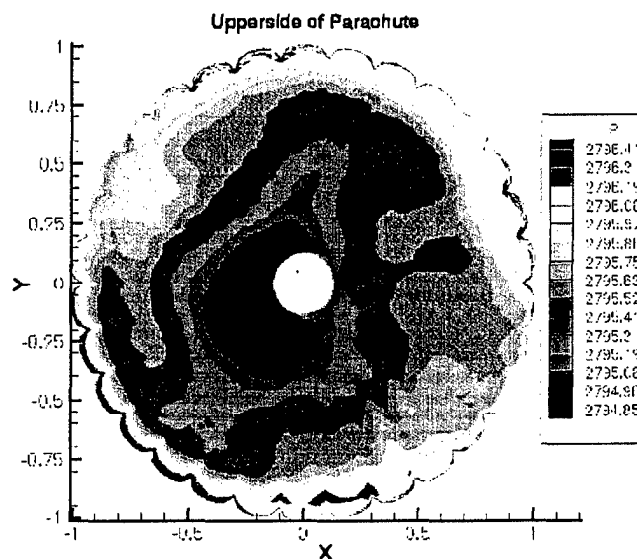


Figure 5. Pressure Contours on the Upper Surface.

The next series of plots shows the comparison of computed pressure contours, velocity magnitudes, and velocity vectors. Computed results obtained from both the finite element and the CFD++ codes are compared. The laminar and the two-equation turbulence model solutions were obtained using the CFD++ code and are compared with the Smagorinsky model solution obtained using the finite element code. Figure 6 shows the pressure contours for these simulations near the parachute. The pressures in the region below the parachute agree rather well between these simulations. As expected, the pressures in the wake region above the parachute are different, especially in the location of the low-pressure regions. It is also clear that all three simulations indicate the flow in the wake to be unsteady. Figures 7 and 8 show the computed velocity magnitude contours and velocity vectors, respectively, on a cut through the xz plane. A certain level of asymmetry is seen in these results. This could be a result of a vortex-shedding type of phenomenon that may arise. Figure 7 shows the flow through the vent hole, which itself seems to be asymmetrical, especially for the solution obtained with the two-equation turbulence model. As seen in this figure, as well as in Figure 8, the flow again is unsteady. The laminar and the two-equation model results indicate two large regions of separated flow in the wake. A couple of smaller bubbles can also be observed near the upper surface of the parachute on both sides of the vent opening. The solution obtained with the Smagorinsky model clearly has many smaller bubbles of recirculatory flow in the wake region. In this case, these results indicate the flow field to be more unsteady than the CFD++ solutions do.

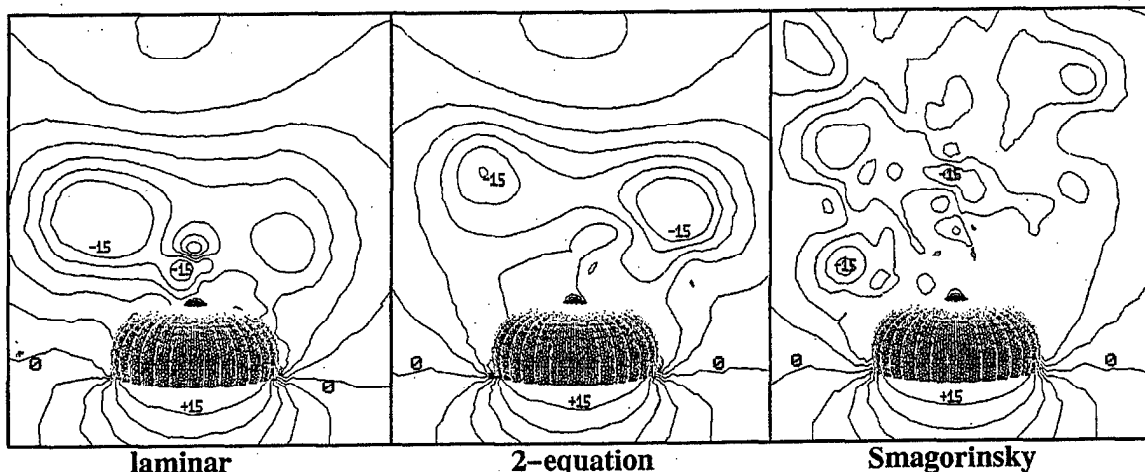


Figure 6. Computed Pressure Contours.

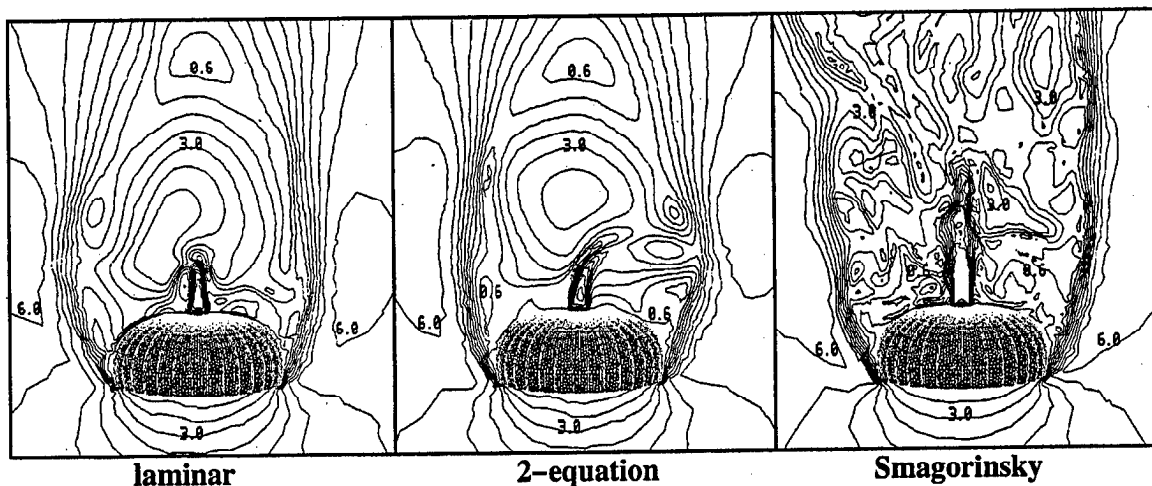


Figure 7. Computed Velocity Magnitude Contours.

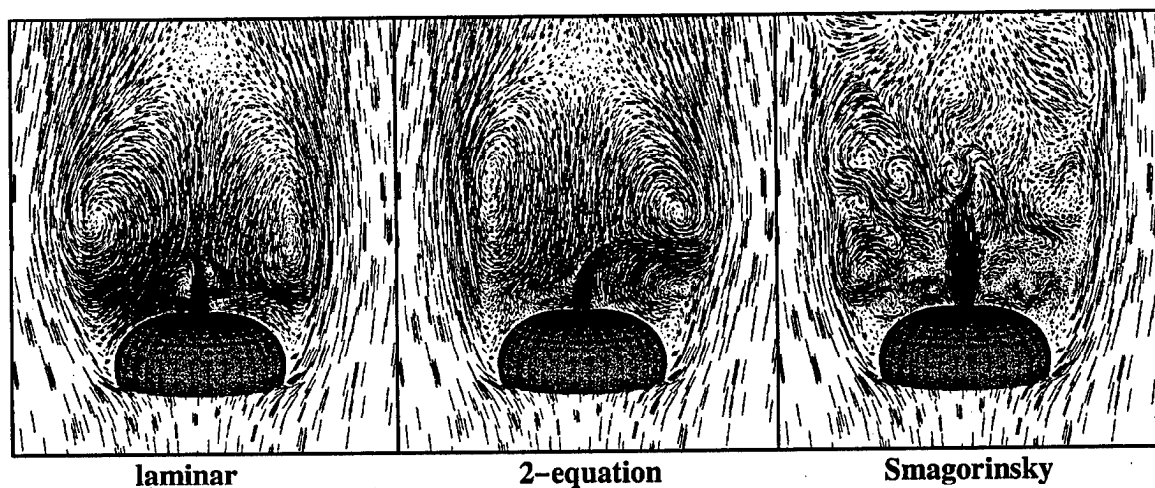


Figure 8. Computed Velocity Vectors.

Figures 9 and 10 show the contours of δp (pressure difference) and δv (velocity-magnitude difference) between various numerical simulations. It is clear that the turbulent simulations differ quite a bit from the laminar solution, especially for the computed pressures in the wake. The two-equation solution seems to be a little closer to the laminar solution in the far wake. Some differences can be observed in the near wake in the velocity magnitudes (see Figure 10). The differences between the Smagorinsky solution and the two-equation model solution may be somewhat larger than the differences between the Smagorinsky solution and the laminar result. Computed results were also obtained for the same case using a one-equation turbulence model. Figure 11 shows the computed pressure contours, velocity magnitude contours, and velocity

vectors for this simulation. The velocity vectors clearly show four bubbles of separated flow regions in the near wake and are quite different from other simulations, especially near the parachute vent opening. Two distinct counter-rotating smaller bubbles can be seen on either side of the flow emerging from the vent opening. Figure 12 shows the δp and δv comparison of this result with the Smagorinsky solution. These differences are generally very similar to those observed in the δp and δv comparison with the two-equation solution.

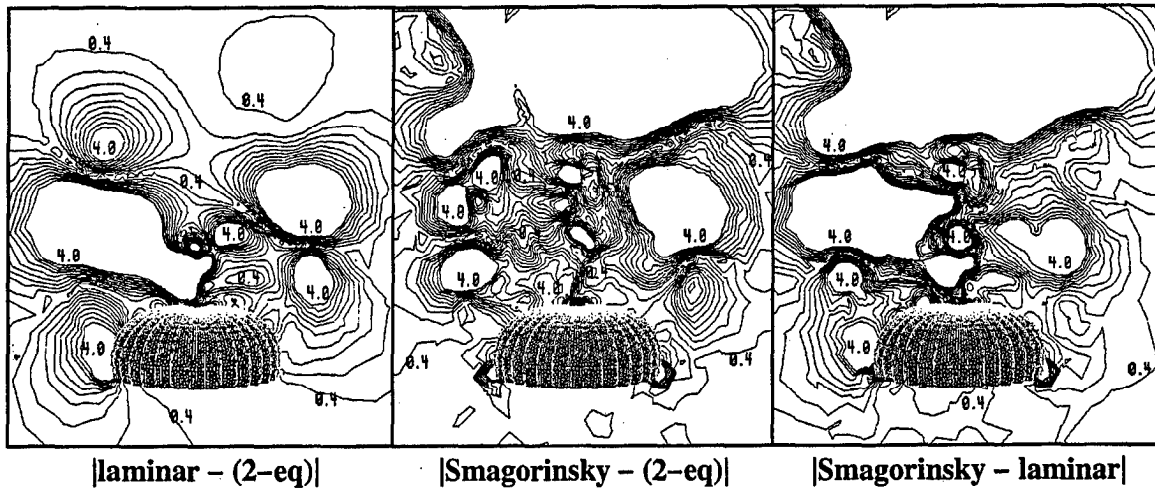


Figure 9. Computed Pressure Comparisons (contours of δp between the simulations).

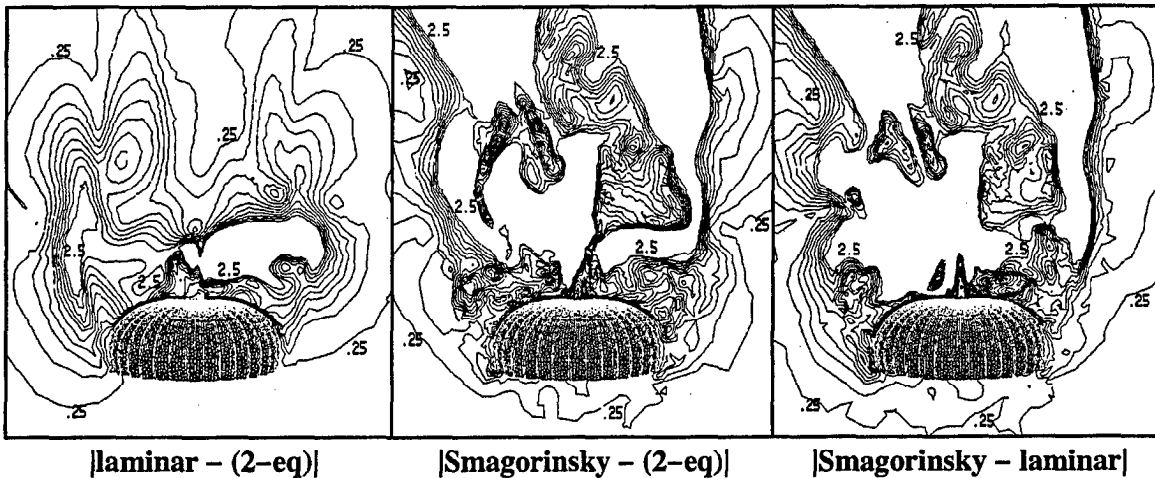


Figure 10. Velocity Magnitude Comparisons (contours of $\delta |v|$ between the simulations).

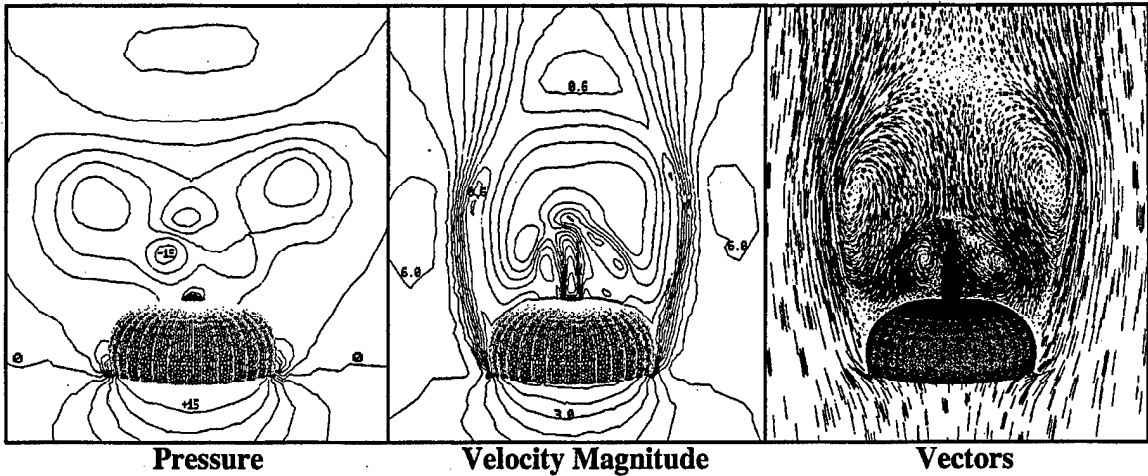


Figure 11. Computed Results With One-Equation Model.

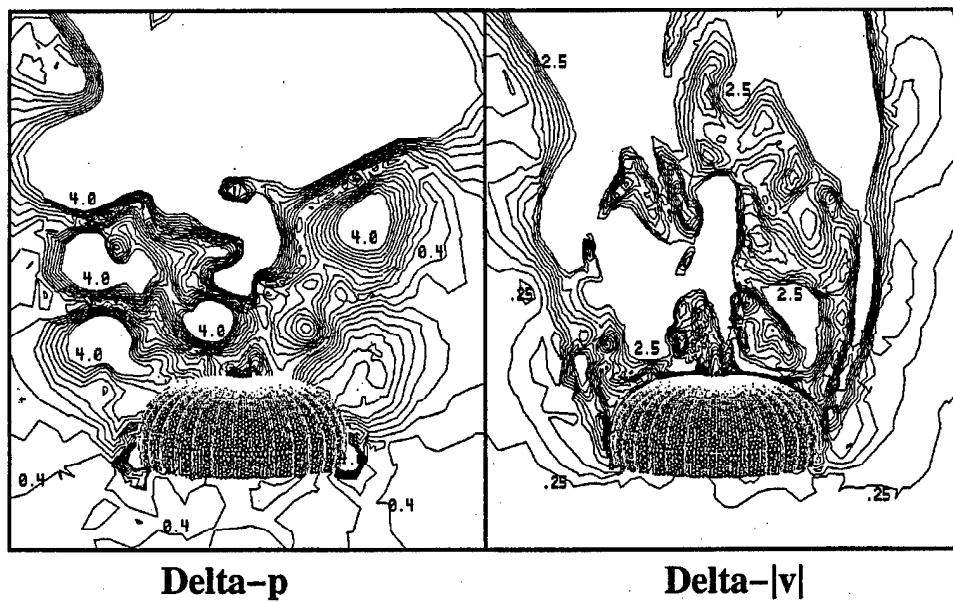


Figure 12. Comparison of Computed Results (Smagorinsky—one-equation model).

Figure 13 shows a time-history plot of non-dimensional drag force obtained with the CFD++ code. Results are shown here for the laminar as well as the one-equation and two-equation turbulence model cases for the same parachute. These results indicate that the flow field is somewhat unsteady. The total aerodynamic drag coefficient, based on a reference area corresponding to a diameter of 35 feet, has been obtained from these computations. The drag coefficients predicted by the laminar, one-equation model, and two-equation model are 0.78, 0.77,

and 0.75, respectively. For comparison, the drag coefficient predicted by the finite element code is 0.89. These results are in reasonably good agreement with the drag coefficient value of 0.79 that can be derived from the actual T-10 system.[17] Some differences do exist in the predicted drag with different numerical techniques. It seems that the turbulence models have a small effect in the prediction of total drag with the type of mesh used here. Also, these results are based on a given shape of the parachute in the terminal state.

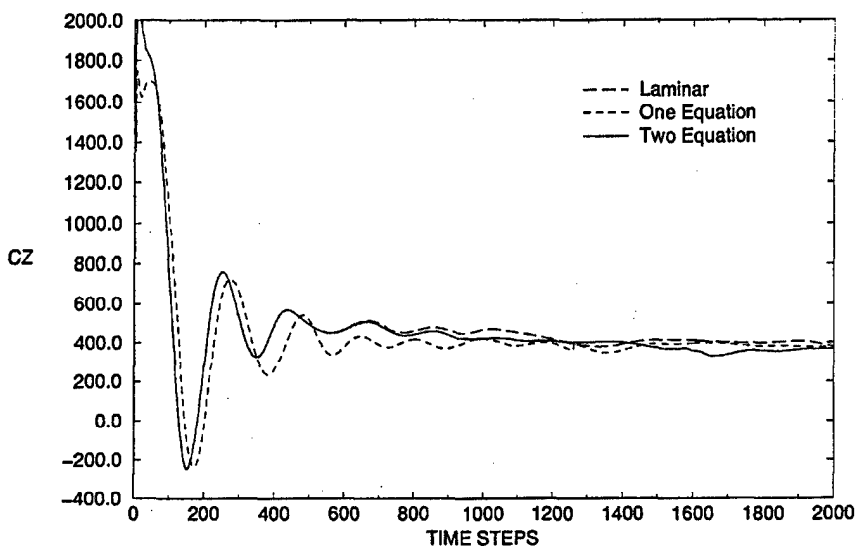


Figure 13. Time History for Drag for T-10 Parachute.

Computations have also been performed on another airdrop system, G12, with and without the payload. All computations for this airdrop system have been performed using the CFD++ code to date. Figure 14 shows the unstructured computational mesh for the G-12 parachute with no payload. This grid (a coarse one) contains 266620 nodes and 1631713 elements. A finer grid (335102 nodes and 2035143 elements) was also generated for the same configuration. Computed results were obtained for both coarse and fine meshes. Figures 15 and 16 show the computed pressure contours for the coarse mesh and the fine mesh, respectively. Qualitative flow features are similar to those observed with the T-10 parachute case (higher pressure on the inside and lower pressures on the outside of the parachute). Figure 17 shows the convergence history of the aerodynamic drag for these computations. It is clear that the coarse mesh solution is more or less steady. On the other hand, the fine mesh solution clearly indicates the flow field to be unsteady. The average drag for the fine mesh case, however, is only 2.5% larger than the drag obtained with the coarse mesh. Figure 18 shows the unstructured mesh about this G-12 canopy, including the payload (in this case, an A-22 container, 4-foot cubed box), and the corresponding computed

pressure contours are shown in Figure 19. The payload affects the incoming flow seen by the parachute. The flow behind the parachute is similar to that of the no-payload case. The flow interference region between the payload and the parachute is quite different from that observed with the no-payload case. Quantitatively, the aerodynamic drag of the G-12 parachute is reduced by about 12% because of the payload. The computed drag coefficients are 0.65 and 0.57 for the G-12 parachute without and with the payload, respectively. For comparison, the drag coefficient derived from the design guide for the G-12 system (total weight of 2,330 lb at a terminal velocity of 28 ft/sec) is 0.78. Note that the CFD computations are for a given shape of the parachute. It is expected that better shapes at the terminal state will result from an FSI simulation, leading to better drag prediction.

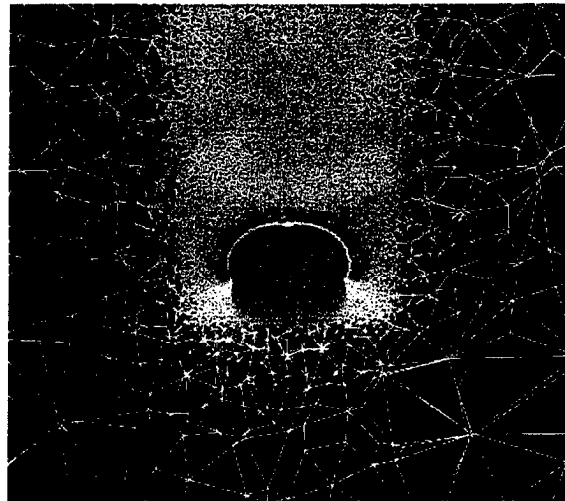


Figure 14. Mesh for G-12 Parachute Without Payload.

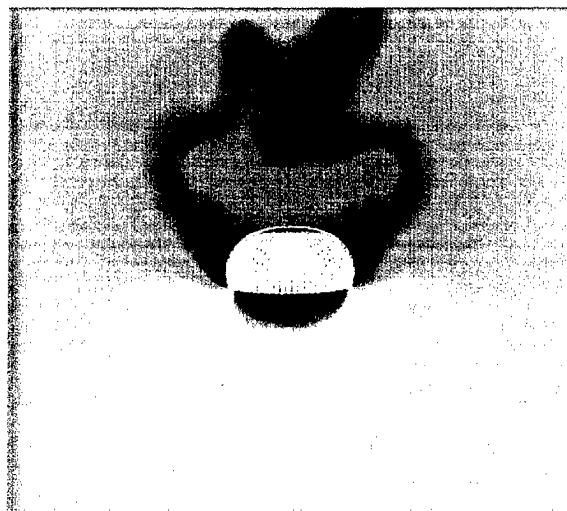


Figure 15. Computed Pressure Contours (coarse mesh).

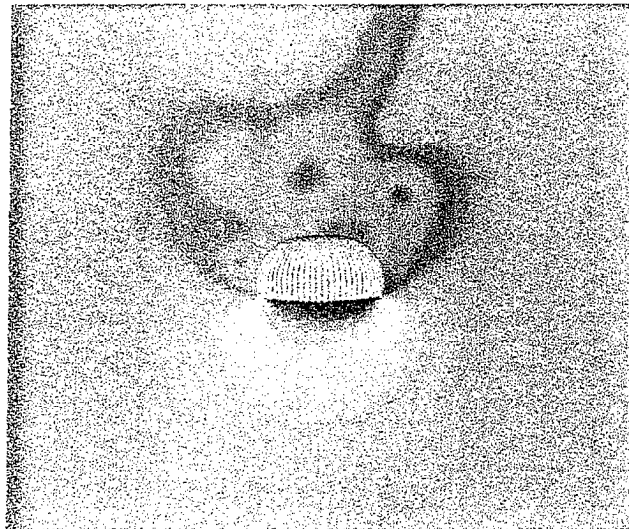


Figure 16. Computed Pressure Contours (fine mesh).

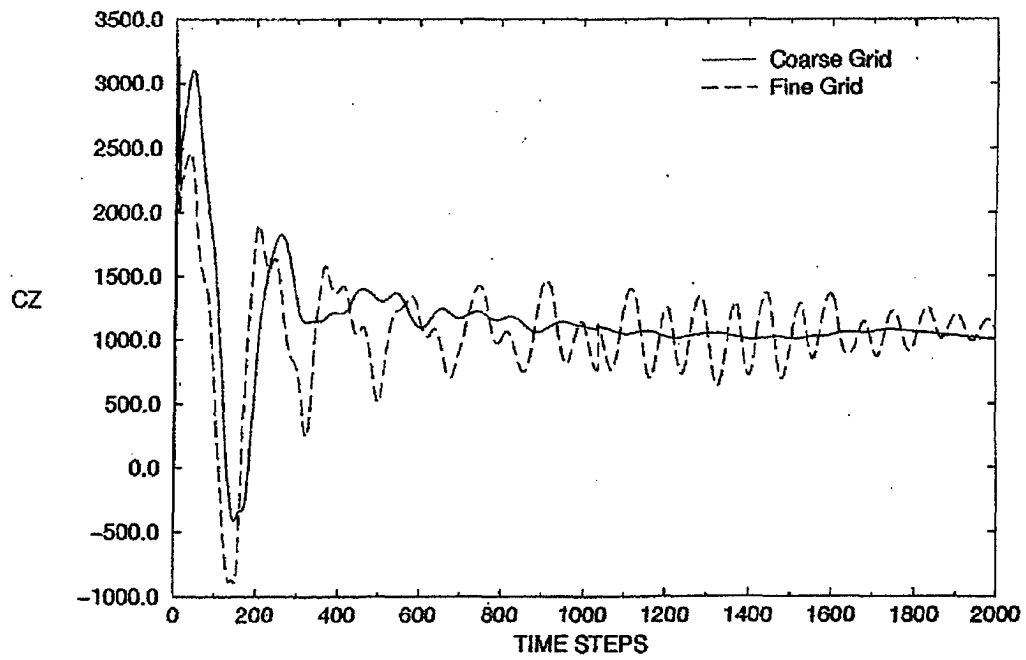


Figure 17. Convergence of Drag for G-12 Canopy.

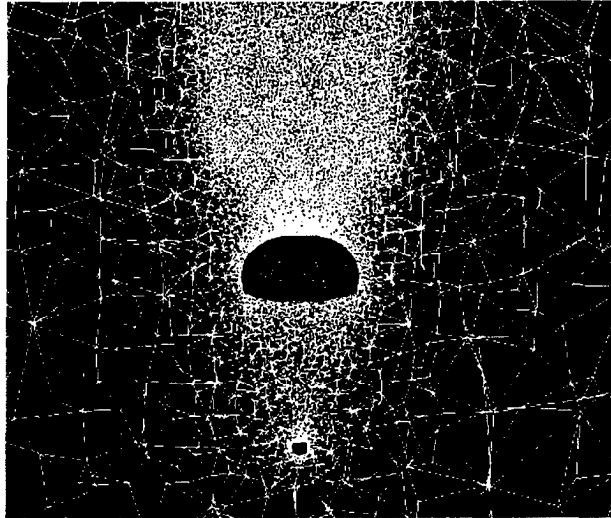


Figure 18. Mesh for G-12 Parachute With Payload.

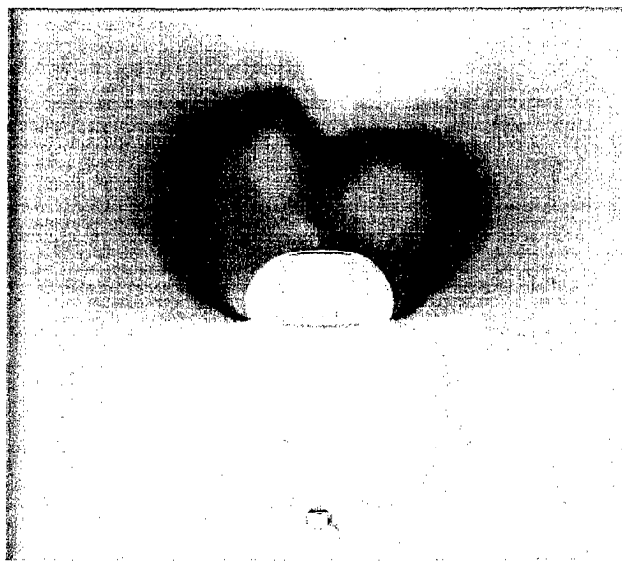


Figure 19. Computed Pressures for G-12 With Payload.

4. CONCLUDING REMARKS

Flow field computations have been performed on two airdrop systems used by the U.S. Army: the T-10 personnel canopy system (no payload) and the G-12 cargo system with and without a payload. Numerical results have been obtained with two different CFD software packages, one based on the stabilized semi-discrete finite element formulation of the incompressible Navier-Stokes equations and the other, a commercially available code, CFD++. For this numerical experiment, computed unsteady flow fields have been obtained with the same

unstructured mesh, and predicted flow fields in and around the parachute are compared. Global quantities such as drag and moment coefficients on the inflated parachute shapes have been obtained from the computed flow field. These forces and moments indicate the unsteady nature of the flow field for the T-10 parachute. Computed results obtained with various turbulence models available with both codes are compared among themselves and with a laminar solution. Most of the differences in the various simulations lie in the near wake of the parachute. The Smagorinsky solution seems to indicate more unsteadiness in the wake region flow field than the other predictions do. Some differences do exist in the predicted drag with different numerical techniques. The flow fields for the G-12 model with and without a payload are also presented. For the G-12 without the payload, the predicted drag is nearly grid independent. The fine mesh solution does show the flow field to be unsteady. Results obtained with the payload show the interference effect in the flow field that reduces the drag of the parachute by about 12%.

REFERENCES

1. Stein, K.R., and R.J. Benney, "Parachute Inflation: A Problem in Aeroelasticity." Technical Report No. NATICK/TR-94/015, U.S. Army Natick Research, Development, and Engineering Center. Natick, MA; August 1994.
2. Sahu, J., G.R. Cooper, and R.J. Benney, "3-D Parachute Descent Analysis Using Coupled CFD and Structural Codes," Proceedings of the 13th AIAA Aerodynamic Decelerator Systems Technology Conference, Clearwater, FL, May 1995.
3. Sahu, J., and R.J. Benney, "Numerical Prediction of Terminal Descent Characteristics of Parachute Clusters Using CFD," AIAA Paper No. 97-1453, June 1997.
4. Lee, C.K., J. Lanza, and J. Buckley, "Apparatus and Method for Measuring Angular Positions of Parachute Canopies," *Journal of Aircraft*, 33(6), 1197-1199, November-December 1996.
5. Tezduyar, T.E., M. Behr, and J. Liou, "A New Strategy for Finite Element Computations Involving Moving Boundaries and Interfaces—the Deforming Spatial-Domain/Space-Time Procedure: I. The Concept And the Preliminary Tests," *Computer Methods in Applied Mechanics and Engineering*, 94, 339-351, 1992.
6. Tezduyar, T.E., M. Behr, S. Mittal, and J. Liou, "A New Strategy for Finite Element Computations Involving Moving Boundaries and Interfaces—the Deforming Spatial-Domain/Space-Time Procedure: II. Computation of Free-Surface Flows, Two Liquid Flows, and Flows With Drifting Cylinders," *Computer Methods in Applied Mechanics and Engineering*, 94, 353-371, 1992.
7. Brooks, W.B., and T.J.R. Hughes, "Streamline Upwind/Petrov-Galerkin Formulations for Convection Dominated Flows With Particular Emphasis on the Incompressible Navier-Stokes Equations," *Computer Methods in Applied Mechanics and Engineering*, 32, 199-259, 1982.
8. Tezduyar, T.E., S. Mittal, S., S.E. Ray, and R. Shih, "Incompressible Flow Computations With Stabilized Bilinear and Linear Equal-Order-Interpolation Velocity-Pressure Elements," *Computer Methods in Applied Mechanics and Engineering*, 95, 221-242, 1992.
9. Smagorinsky, J., "General Circulation Experiments With the Primitive Equations," *Monthly Weather Review*, 91, 99-165, 1963.
10. Peroomian, O., S.R. Chakravarthy, S. Palaniswamy, and U.C. Goldberg, "Convergence Acceleration for Unified-Grid Formulation Using Preconditioned Implicit Relaxation," AIAA Paper No. 98-0116, 1998.
11. Goldberg, U.C., O. Peroomian, and S.R. Chakravarthy, "A Wall-Distance-Free K-E Model with Enhanced Near-Wall Treatment," *ASME Journal of Fluids Engineering*, 120, 457-462, 1998.

12. Weiss, J.M., and W.A. Smith, "Preconditioning Applied to Variable and Constant Density Flows," AIAA Journal, 33(11), 1995.
13. Turkel, E., A. Fiterman, and B. Van-Leer, "Preconditioning and the Limit to the Incompressible Flow Equations," Institute for Computer Applications in Science and Engineering (ICASE), Report 93-42, Hampton, VA, 1993.
14. Benney, R.J., and J.W. Leonard, "A 3-D Finite Element Structural Parachute Model," Proceedings of the 13th AIAA Aerodynamic Decelerator Systems Technology Conference, Clearwater, FL, May 1995.
15. Benney, R.J., K.R. Stein, J.W. Leonard, and M.L. Accorsi, "Current 3-D Structural Dynamic Finite Element Modeling Capabilities," Proceedings of the 14th AIAA Aerodynamic Decelerator Systems Technology Conference, San Francisco, CA, May 1997.
16. Johnson, A.A., and T.E. Tezduyar, "Parallel Computation of Incompressible Flows With Complex Geometries," International Journal for Numerical Methods in Fluids, 24, 1321-1340, 1997.
17. Ewing, E.G., H.W. Bixby, and T.W. Knacke, "Recovery Systems Design Guide," Technical Report AFFDL-TR-78-151, U.S. Air Force Flight Dynamics Laboratory, December 1978.

<u>NO. OF COPIES</u>	<u>ORGANIZATION</u>	<u>NO. OF COPIES</u>	<u>ORGANIZATION</u>
2	ADMINISTRATOR DEFENSE TECHNICAL INFO CENTER ATTN DTIC OCP 8725 JOHN J KINGMAN RD STE 0944 FT BELVOIR VA 22060-6218	1	CDR NSWC CODE 420 DR A WARDLAW INDIAN HEAD MD 20640-5035
1	DIRECTOR US ARMY RESEARCH LABORATORY ATTN AMSRL CS AL TA REC MGMT 2800 POWDER MILL RD ADELPHI MD 20783-1197	1	CDR NSWC ATTN DR F MOORE DAHLGREN VA 22448
1	DIRECTOR US ARMY RESEARCH LABORATORY ATTN AMSRL CI LL TECH LIB 2800 POWDER MILL RD ADELPHI MD 207830-1197	1	NAVAL AIR WARFARE CENTER ATTN DAVID FINDLAY MS 3 BLDG 2187 PATUXENT RIVER MD 20670
1	DIRECTOR US ARMY RESEARCH LABORATORY ATTN AMSRL DD J J ROCCHIO 2800 POWDER MILL RD ADELPHI MD 20783-1197	4	DIR NASA LANGLEY RESEARCH CENTER ATTN TECH LIBRARY MR D M BUSHNELL DR M J HEMSCH DR J SOUTH LANGLEY STATION HAMPTON VA 23665
7	CDR US ARMY ARDEC ATTN AMSTE AET A R DEKLEINE C NG R BOTTICELLI H HUDGINS J GRAU S KAHN W KOENIG PICATINNY ARSENAL NJ 07806-5001	2	ARPA ATTN DR P KEMMEY DR JAMES RICHARDSON 3701 NORTH FAIRFAX DR ARLINGTON VA 22203-1714
1	CDR US ARMY ARDEC ATTN AMSTE CCH V PAUL VALENTI PICATINNY ARSENAL NJ 07806-5001	7	DIR NASA AMES RESEARCH CENTER MS 227 8 L SCHIFF MS 258 1 T HOLST MS 258 1 D CHAUSSEE MS 258 1 M RAI MS 258 1 P KUTLER MS 258 1 P BUNING MS 258 1 B MEAKIN MOFFETT FIELD CA 94035
1	CDR US ARMY ARDEC ATTN SFAE FAS SD MIKE DEVINE PICATINNY ARSENAL NJ 07806-5001	2	USMA DEPT OF MECHANICS ATTN LTC ANDREW L DULL M COSTELLO WEST POINT NY 10996
2	USAF WRIGHT AERONAUTICAL LABS ATTN AFWAL FIMG DR J SHANG MR N E SCAGGS WPAFB OH 45433-6553	2	UNIV OF CALIFORNIA DAVIS DEPT OF MECHANICAL ENGRG ATTN PROF H A DWYER PROF M HAFEZ DAVIS CA 95616
3	AIR FORCE ARMAMENT LAB ATTN AFATL/FXA STEPHEN C KORN BRUCE SIMPSON DAVE BELK EGLIN AIR FORCE BASE FL 32542-5434		
1	CDR NSWC CODE B40 DR W YANTA DAHLGREN VA 22448-5100		

<u>NO. OF COPIES</u>	<u>ORGANIZATION</u>	<u>NO. OF COPIES</u>	<u>ORGANIZATION</u>
1	AEROJET ELECTRONICS PLANT ATTN DANIEL W PILLASCH B170 DEPT 5311 PO BOX 296 1100 WEST HOLLYVALE STREET AZUSA CA 91702	1	UNIVERSITY OF MARYLAND DEPT OF AEROSPACE ENGRG ATTN DR J D ANDERSON JR COLLEGE PARK MD 20742
1	MIT TECH LIBRARY 77 MASSACHUSETTS AVE CAMBRIDGE MA 02139	1	UNIVERSITY OF NOTRE DAME DEPT OF AERONAUTICAL & MECH ENGRG ATTN PROF T J MUELLER NOTRE DAME IN 46556
1	GRUMANN AEROSPACE CORP AEROPHYSICS RESEARCH DEPT ATTN DR R E MELNIK BETHPAGE NY 11714	1	UNIVERSITY OF TEXAS DEPT OF AEROSPACE ENGRG MECH ATTN DR D S DOLLING AUSTIN TX 78712-1055
2	MICRO CRAFT INC ATTN DR JOHN BENEK NORMAN SUHS 207 BIG SPRINGS AVE TULLAHOMA TN 37388-0370	1	UNIVERSITY OF DELAWARE DEPT OF MECHANICAL ENGRG ATTN DR JOHN MEAKIN NEWARK DE 19716
1	LANL ATTN MR BILL HOGAN MS G770 LOS ALAMOS NM 87545	4	COMMANDER USAAMCOM ATTN AMSAM RD SS AT ERIC KREEGER GEORGE LANDINGHAM CLARK D MIKKELSON ED VAUGHN REDSTONE ARSENAL AL 35898-5252
1	METACOMP TECHNOLOGIES INC ATTN S R CHAKRAVARTHY 650 HAMPSHIRE ROAD SUITE 200 WESTLAKE VILLAGE CA 91361-2510	4	LOCKHEED MARTIN VOUGHT SYS PO BOX 65003 M/S EM 55 ATTN PERRY WOODEN W B BROOKS JENNIE FOX ED MCQUILLEN DALLAS TX 75265-0003
2	ROCKWELL SCIENCE CENTER ATTN S V RAMAKRISHNAN V V SHANKAR 1049 CAMINO DOS RIOS THOUSAND OAKS CA 91360	1	COMMANDER US ARMY TACOM-ARDEC BLDG 162S ATTN AMCPM DS MO PETER J BURKE PICATINNY ARSENAL NJ 07806-5000
1	ADVANCED TECHNOLOGY CTR ARVIN/CALSPAN AERODYNAMICS RESEARCH DEPT ATTN DR M S HOLDEN PO BOX 400 BUFFALO NY 14225	3	COMMANDER US ARMY SOLDIER & BIOLOGICAL CHEMICAL COMMAND SOLDIER SYSTEMS CENTER ATTN R BENNEY K STEIN C LEE NATICK MA 01760-5017
1	UNIV OF ILLINOIS AT URBANA CHAMPAIGN DEPT OF MECH & IND ENGINEERING ATTN DR J C DUTTON URBANA IL 61801		<u>ABERDEEN PROVING GROUND</u>
		2	DIRECTOR US ARMY RESEARCH LABORATORY ATTN AMSRL CI LP (TECH LIB) BLDG 305 APG AA

<u>NO. OF COPIES</u>	<u>ORGANIZATION</u>	<u>NO. OF COPIES</u>	<u>ORGANIZATION</u>
2	CDR US ARMY ARDEC FIRING TABLES BRANCH ATTN R LIESKE R EITMILLER F MIRABELLE BLDG 120	3	DIR USARL AMSRL WM BE G WREN M NUSCA J DESPIRITO BLDG 390
1	DIR USARL ATTN AMSRL CI C NIETUBICZ BLDG 394	1	DIR USARL ATTN AMSRL WM BF J LACETERA BLDG 120
2	DIR USARL ATTN AMSRL CI H D HISLEY D PRESSEL BLDG 394		<u>ABSTRACT ONLY</u>
1	DIR USARL ATTN AMSRL CI H W STUREK BLDG 328	1	DIRECTOR US ARMY RESEARCH LABORATORY ATTN AMSRL CS AL TP TECH PUB BR 2800 POWDER MILL RD ADELPHI MD 20783-1197
2	DIR USARL ATTN AMSRL WM I MAY L JOHNSON BLDG 4600		
3	DIR USARL ATTN AMSRL WM B A W HORST JR W CIEPIELLA E M SCHMIDT BLDG 4600		
7	DIR ARL ATTN AMSRL WM BA W D'AMICO F BRANDON T BROWN L BURKE J CONDON B DAVIS M HOLLIS BLDG 4600		
16	DIR USARL ATTN AMSRL WM BC P PLOSTINS M BUNDY G COOPER H EDGE J GARNER B GUIDOS K HEAVEY D LYON A MIKHAIL V OSKAY J SAHU K SOENCKSEN D WEBB P WEINACHT S WILKERSON A ZIELINSKI BLDG 390		
1	DIR USARL ATTN AMSRL WM BD B FORCH BLDG 4600		

INTENTIONALLY LEFT BLANK

